Title
Pyroptosis by caspase11/4-gasdermin-D pathway in alcoholic hepatitis in mice and patients

Journal
Hepatology, 67(5)

ISSN
0270-9139

Authors
Khanova, Elena
Wu, Raymond
Wang, Wen
et al.

Publication Date
2018-05-01

DOI
10.1002/hep.29645

Peer reviewed

HHS Public Access

Author manuscript

Hepatology. Author manuscript; available in PMC 2019 May 01.

Published in final edited form as:

Hepatology. 2018 May ; 67(5): 1737–1753. doi:10.1002/hep.29645.

Pyroptosis by Caspase11/4-Gasdermin-D Pathway in Alcoholic Hepatitis

Elena Khanova[1], **Raymond Wu**[1], **Wen Wang**[1], **Rui Yan**[1], **Yibu Chen**[2], **Samuel W. French**[3], **Cristina Llorente**[4], **Stephanie Q. Pan**[1], **Qihong Yang**[1], **Yuchang Li**[1], **Raul Lazaro**[1], **Charles Ansong**[5], **Richard D. Smith**[5], **Ramon Bataller**[6], **Timothy Morgan**[7], **Bernd Schnabl**[4], and **Hidekazu Tsukamoto**[1,8]

[1]Southern California Research Center for ALPD and Cirrhosis and Department of Pathology, Los Angeles, California, USA

[2]Bioinformatics Service, Keck School of Medicine of the University of Southern California, Los Angeles, California, USA

[3]Harbor-UCLA Medical Center, Torrance, California, USA

[4]Department of Medicine, University of California San Diego and VA San Diego Healthcare System, San Diego, California, USA

[5]Pacific Northwest National Laboratory, Richland, WA 99352

[6]Division of Gastroenterology, Hepatology and Nutrition, Department of Medicine, University of Pittsburgh, Pittsburgh, Pennsylvania, USA

[7]Gastroenterology Services, VA Long Beach Healthcare System, Long Beach, California, USA

[8]Department of Veterans Affairs Greater Los Angeles Healthcare System, Los Angeles, California, USA

Abstract

Alcoholic hepatitis (AH) continues to be a disease with high mortality and no efficacious medical treatment. Although severe AH is presented as acute on chronic liver failure, what underlies this transition from chronic alcoholic steatohepatitis (ASH) to AH, is largely unknown. To address this question, unbiased RNA-seq and proteomic analyses were performed on livers of the recently developed AH mouse model which exhibits the shift to AH from chronic ASH upon weekly alcohol binge, and these results are compared with gene expression profiling data from AH patients. This cross-analysis has identified *Casp11* (*CASP4* in man) as a commonly upregulated gene known to be involved in non-canonical inflammasome pathway. Immunoblotting confirms

Correspondence to: Hidekazu Tsukamoto, 1333 San Pablo Street MMR-402, Los Angeles, CA 90033, USA, tel: 323-442-5107, fax: 323-442-3126, htsukamo@med.usc.edu.

Author contributions: H.T. conceived the overall project, designed all experiments, interpreted all data and wrote the manuscript with input from other authors. R.L., Q.Y., and Y.L. performed animal experiments; E.K, W.W., and R.W. performed biochemical analyses; S.W.F. performed histological analysis; Y.C. performed bioinformatics analysis; C.L. performed bacterial PCR analysis; S.Q.P isolated hepatocytes and hepatic macrophages from the AH mouse model; Q.Y., Y.L., and R.L. performed all mouse experiments; B.S. supervised bacterial PCR analysis and advised the senior author on its interpretation; R.B. provided microarray data on AH patient livers; C.A. and R.D.S. performed proteomic analysis; T.M. advised the senior author and supported collaboration with his research consortium investigators.

CASP11/4 activation in AH mice and patients but not in chronic ASH mice and healthy human livers. Gasdermin-D (GSDMD) which induces pyroptosis (lytic cell death caused by bacterial infection) downstream of CASP11/4 activation, is also activated in AH livers in mice and patients. CASP11 deficiency reduces GSDMD activation, bacterial load in the liver, and the severity of AH in the mouse model. Conversely, the deficiency of IL-18, the key anti-microbial cytokine, aggravates hepatic bacterial load, GSDMD activation, and AH. Further, hepatocyte-specific expression of constitutively active GSDMD worsens hepatocellular lytic death and PMN inflammation. These results implicate pyroptosis induced by CASP11/4-GSDMD pathway in the pathogenesis of AH.

Keywords

IL-18; non-canonical inflammasome; bacterial translocation

Alcohol hepatitis (AH) is a unique spectrum of alcoholic liver disease (ALD) with high short-term mortality as high as 50% and with limited efficacious medical treatments (1). It is acute-on-chronic liver disease characterized by hepatic steatosis, ballooned hepatocytes with Mallory-Denk bodies, neutrophilic infiltration and liver fibrosis or cirrhosis, and clinically presented with de-compensated liver functions with cholestasis, hypoalubuminemia, coagulopathy, portal hypertension (2). Patients with severe AH develop sepsis, liver failure, and multiorgan dysfunction leading to rapid progression to death. Common treatments for AH include prednisolone and pentoxyfiline that are primarily aimed to suppress inflammation. But their outcome are still controversial, due to an inherent risk of increasing infection by the corticosteroid and to suppression of regenerative effects of TNFα by pentoxifyline (3). Nutritional therapy to supplement calories and protein has been attempted but its efficacy is variable among the patients. Liver transplantation is successfully performed for AH patients which improves short and long-term survival (4, 5), but it requires collective and coordinated efforts of hepatologist, surgeon, addiction specialist, and social worker, as well as the prolonged abstinence often required for transplantation in the U.S. which is realistically difficult for patients with severe AH who are expected to have high short-term mortality.

Obviously, hepatocytes are the primary target of alcohol effects. Research during the past 3 decades has indeed disclosed several key mechanisms of alcohol-mediated hepatocellular damage including CYP2E1-mediated oxidant stress, mitochondrial glutathione stress, endoplasmic reticulum (ER) stress, malondialdehyde-acetaldehyde protein adducts, centrilobular hypoxia, suppressed autophagy and lysosomal dysfunction to list a few (6–8). These mechanisms may likely co-exist and synergistically promote cellular injury via sensitization of hepatocytes and priming of hepatocytes and other cell types, culminating to hepatocellular death characterized by apoptosis, necrosis or necroptosis. However, these mechanistic events are primarily identified in animal models which only produce fatty liver or mild steatohepatitis, and whether they are directly relevant to the pathogenesis of AH is unknown. To design logical therapeutic modalities for AH, this presents a major obstacle. Another problem is the lack of information as to what chronic precursor lesions exist prior to developing acute-on-chronic pathology in AH patients. This knowledge gap stems from our

inability to access and study asymptomatic chronic alcoholic steatohepatitis (ASH) patients as recently addressed (1, 9). Difficulties in reproducing the histology and clinical features of AH in animal models have undoubtedly been a major limiting factor for our progress in addressing these questions. However, recent developments of the mouse models with superimposing binge alcohol administration, allowed reproduction of neutrophilic infiltration and aggravated liver pathology (10–13). In particular, we have developed so-called hybrid feeding mouse model which incorporated *ad libitum* feeding of the Western diet into the intragastric ethanol diet feeding which assures sustained high alcohol intake and intoxication (12). This model develops chronic ASH accompanied by macrophage activation and pericellular and perisinusoidal liver fibrosis. Moreover, weekly binge in this model shifts inflammation to neutrophilic infiltration and induces ductular reaction, as seen in patients with AH, and some of clinical features of AH such as splenomegaly, hypoalbuminemia, and increased plasma bilirubin levels (12). This hybrid feeding model with or without binge, thus provides a unique opportunity to investigate the mediators responsible for an acute-on-chronic phenotype of AH. To this end, we have applied a global unbiased RNA-seq and proteomic analyses, and published gene profiling data from AH patient livers (14) vs. normal livers, were integrated to identify commonly regulated genes in the mouse model and AH patients. This pursuit identifies *Casp11* (for mouse)/*CASP4* (for human) as an upregulated gene in both the mouse model and patients. CASP11 activation is evident in AH livers in both mice and patients and accompanied by increased activation of Gasdermin-D (GSDMD), the recently discovered effector for pyroptosis, suicidal death of the cells infected with bacteria. Loss and gain of function manipulations for CASP11 and/or GSDMD confirm its importance in controlling bacterial infection and induction of AH in the model.

Materials and Methods

Mice and cells

Male C57BL/6j, B6.129S4(D2)-*Casp4tm1Yuan*/J, B6.129P2-*Il18tm1Aki*/J mice were subjected to the AH regimen as previously described (12). It consists of 2 weeks of *ad libitum* feeding of chow or diet high in cholesterol and saturated fat (HCFD) (Dyets Inc. #180529), surgical implantation of intragatric (iG) catheter, 1-wk acclimatization with iG feeding of a control high fat diet (corn oil, 36%Cal) for 60% of daily caloric requirement and *ad libitum* feeding of HCFD or chow for the remaining 40%Cal, and switching to an ethanol high fat diet with incrementally increasing ethanol concentration over a 8-wk period for ethanol-fed mice. This hybrid feeding regimen produces chronic ASH, and superimposition of weekly ethanol binge shifts liver pathology to AH. For AH mice, ethanol binge was given weekly from the 2nd week by withdrawing ethanol infusion for 5–6 hours before and after the binge and administering an equivalent amount of ethanol withdrawn as a bolus (4~5g/kg). For control mice, isocaloric dextrose was given as a bolus in the identical manner. Hepatocytes and hepatic macrophages were isolated by a standard collagenase perfusion and cultured 2 hours on collagen-coated dish for extraction of proteins. Raw264.7 cells were electroporated with an increasing concentration of LPS (0.125–5μg/ml) without or with CASP11/4 inhibitor (Santa Cruz Biotech.) by Neon™ Transfection System (Invitrogen) and cultured 3–18 hr before protein extraction.

RNA extraction and RT-qPCR

Total RNA was extracted from liver tissues by Quick-RNA MiniPrep (Zymo Research) or Direct-zol RNA MiniPrep Kit (Zymo Research). For RT-qPCR, cDNAs were synthesized from 1 μg total RNA using the Maxima First Strand Synthesis Kit for RT-qPCR (Thermo Scientific). Quantitative PCR was performed by amplifying cDNA for 40 cycles using the SYBR Green PCR master mix (Applied Biosystems) and the ViiA 7 Real-Time PCR System (Applied Biosystems). Each threshold cycle (Ct) value was first normalized to the 36B4 (Rplp0) Ct value of a sample and subsequently to a control sample. Primers used are shown in Supplemental Methods -Table 1.

RNA-seq and proteomic analysis

RNA samples were provided to the USC Genomics Core for library construction and sequencing. Library construction was carried out using the Illumina TruSeq RNA Sample Prep kit. Libraries were applied to an Illumina flow cell and run on the Illumina HiSeq 2000 as a single-end read for 50 cycles with total raw reads per sample averaged around 22 millions. RNA-seq data was analyzed with Partek Flow version 4 (Partek Inc., St. Louis, MO). Raw sequencing reads were first trimmed from both ends with Quality Score method and then mapped to the mouse genome mm10 using Tophat version 2.0.5 (15) with default parameter settings and using Gencode M2 annotation (16). Read counts per gene/transcript in all samples were normalized using Upper Quartile normalization (17) and analyzed for differential expression by Partek Gene Specific Analysis method. The differentially expressed gene (DEG) lists were generated for each comparison using the cutoff of FDR<0.05 and fold changes greater than 2 either direction. Hierarchical clustering of samples based on DEG lists was carried out using Partek Genomic Suite version 5. Downstream functional analysis of the DEG lists were carried out using Ingenuity Pathway System (Qiagen, Redwood City CA). Hepatic gene expression profiling was also assessed in patients with AH (n-15) and normal livers (n=7) by DNA microarray as previously described (14). All AH patients had transjugular liver biopsy and histological diagnosis of AH. They had the Maddrey's discriminant function of 59+6 and bilirubin of 12.5+1.21 mg/dl with 77% of them defined as having severe AH based on ABIC (Age-Bilirubin-INR-Creatinine score) score >6.71 (14). Proteomics sample preparation and mass spectrometry analysis was performed with an LTQ-Orbitrap-Velos mass spectrometer (Thermo Scientific) as previously described (18).

Immunoblot analysis, CASP4/11 assay and cytokine ELISA

Mouse liver proteins were extracted with RIPA buffer (Santa Cruz Biotechnology). AH patient and control human livers were obtained from the Clinical Resources for Alcoholic Hepatitis Investigators (1R24AA025017) of Johns Hopkins University. These tissues were excised from explanted livers in patients with severe alcoholic hepatitis during liver transplantation, or wedge biopsies from the donor livers (normal control). Supplementary Result - Table 5 summarizes basic clinical information of 5 AH patients and 5 healthy donors. For GASMD immunoblot, the membrane and cytosolic proteins were isolated by using Mem-PER™ Plus Membrane Protein Extraction kit (Thermo Scientific). Twenty~40μg proteins were mixed with 6x SDS sample buffer, resolved by 6%–10% SDS-

PAGE, transferred onto PVDF membrane, and immunoblotted. The sources and dilutions of primary antibodies used were: CASP1 (sc-514, Santa Crutz Biotech., x500), CASP11/4 (M029-3, MBL, x500), IL-1β (#30311, R&D System, x500), GSDMD (G7422, Sigma-Aldrich, x500). CASP11/4 activity was determined in liver homogenate supernatant by a kit which uses the LEVD substrate cleavage motif (Abcam). This assay has some cross-reactivity with CASP5 but not with CASP1-3 or 6-10. IL-1 and IL-18 concentrations were determined in plasma or liver homogenate supernatant by ELISA (R&D System and MBL).

Histological analysis, morphometric analysis, and plasma chemistry

Left, middle, and right liver lobes were sliced, fixed with 3% paraformaldehyde, and processed for paraffin embedding by Histology Core of the USC Research Center for Liver Diseases (P30DK048522) and H&E staining by the Morphology Core of the Southern California Research Center for ALPD and Cirrhosis for blind analysis. Histological grading was performed for macro- and micro-vesicular steatosis, liver necrosis, MNC and PMN inflammation, lipogranuloma, and fibrosis. In brief, 1+, 2+, 3+, and 4+ are assigned for micro- or macro-vesicular steatosis based on <25%, 25–49%, 50–74%, 75–100% of cells with respective type of steatosis. MNC and PMN inflammation were graded as 1+, 2+, 3+ if each low power view contains 1–2, 3–7, more than 7 foci of infiltration, respectively and 4+ was assigned if every lobule contained several foci. PMN infiltrated into the parenchyma were counted on stained liver sections of the three major lobes and expressed per $100mm^2$. The numbers of hepatocytes undergoing lytic death vs. surviving cells were counted over 5 views under ×200 magnification in three different lobes and expressed as the percent of dead hepatocytes. Immunostaining for ductular reaction/oval cells was performed using OV-6 antibody (Santa Cruz, sc-101863). Plasma chemistry such as ALT, AST, alkaline phosphatase, bile acids were determined by ANTECH Diagnostics by using autoanalyzer.

Bacterial DNA isolation and qPCR

A small portion of right liver lobe (~150mg) was aseptically removed for genomic DNA extraction. The qPCR was performed for 16S rRNA bacterial universal sequence and normalized to host 18S rRNA as previously performed (19).

Adeno-associated virus-mediated expression

AAV serotype 8 was used to construct the vector which drives expression of active mouse GSDMD (aa1-276) under the hepatocyte-specific Ttr promoter (Vector Biolab), and AAV-Ttr-eGFP was used as a control. Each mouse received 5×10e11 GC of either AAV vector in100μl PBS via tail vein during the acclimatization period after the intragastric catheter implantation.

Statistics

All numerical data are expressed as the means and standard error (SEM) and the statistical significance of a difference between the two sets of data or among different groups was analyzed by student t-test or ANOVA.

Results

Comparative transcriptome analysis in AH in mice and patients

The hybrid feeding combining *ad libitum* consumption of the Western diet which is prevalent among AH patients and intragastric feeding of ethanol containing diet which assures high intake of ethanol as seen in human alcoholics, results in induction of chronic ASH (cASH) with macrophage infiltration and liver fibrosis as previously shown (12). Superimposing this regimen with weekly alcohol binge, shifts liver pathology to alcoholic hepatitis with neutrophilic infiltration (herein abbreviated as AH) despite equal overall alcohol intake (12). To identify novel mediators for the pathogenesis of AH, we have performed transcriptome analysis by RNA-seq and proteomic analysis on the livers of cASH and AH mice and compared to control mice (Control) with isocaloric hybrid feeding of chow and intragastric control liquid diet. These results were compared to liver microarray data on AH patient vs. control subjects as previously reported (10). As the patient data do not have a group representing chronic ASH, we first compared differentially regulated genes in AH patients vs. control subjects with differentially regulated genes and proteins in AH mice vs. control mice (Fig. 1C). As shown in Venn diagrams, approximately 25% and 17% of upregulated and downregulated genes in mouse AH are also shared by patient AH data, respectively. Comparing RNA-seq and proteomic data from mice, only 7.8% and 7.3% of upregulated and down-regulated genes are included in the protein data respectively (the lists shown in Suppl. Table 1 and 2) while 37.5% and 68.2% of upregulated and down-regulated proteins are also differentially regulated at the mRNA level. This is likely due to a number of factors including the higher coverage obtained by RNA-seq analysis compared to proteomics analysis and well appreciated post-transcriptional mechanisms (20) which results in the low percentages of the former set of comparison. suggesting the low sensitivity of proteomic analysis which results in the low percentages of the former set of comparison. Differentially regulated genes in AH vs. control in both the mouse model and patients were subjected to Ingenuity Pathway Analysis. This analysis identifies genes implicated in cancer, cardiovascular disease, inflammation, organ injury, and immunologic disease, are upregulated in both the mouse model and patients in the manner suggestive of induced pathways for mitochondrial stress, cell death, inflammation, liver fibrosis, and cell cycle/DNA damage which are expected in AH (Fig. 1D). Commonly down-regulated genes in AH mice and patients, are functionally categorized into FXR, LXR, CAR, and PXR activation involved in bile acid, fatty acid, and xenobiotic metabolism (Fig. 1E), suggesting impaired hepatocellular metabolic activities expected from failing livers in AH. These results represent transcriptome data-based confirmation of the important features of clinical AH reproduced by the mouse model.

Next we asked what genes are differentially regulated in mouse AH vs. cASH to identify potential driver genes for the transition from cASH to AH. This analysis shows 495 upregulated and 465 down-regulated genes in AH as compared to cASH, and 19.8% (98 genes) and 28.2% (131 genes) of these genes are also identified in the AH patient data compared to control subjects (Fig. 1F, Suppl. Table 3 and 4). Again, the concordance rate for differentially regulated proteins in the mouse model is relatively poor for these commonly upregulated genes in AH mice likely due to the relatively lower coverage of the proteomic

analysis. Ontology and pathway analysis of 98 commonly upregulated genes, reveals several functional categories for which many genes are induced, such as chemokine signaling, inflammasome activation, cell death, and fibrosis which are expected from more pronounced inflammatory and fibrotic changes observed in AH (Table 1). From these data, we are intrigued by two results: 1) genes involved in the pathway activated by bacterial infection are upregulated in both mice and patients; and 2) *Casp11/4*, which is involved in activation of non-canonical inflammasome and pyroptosis in response to bacterial infection (21), is commonly upregulated in AH mice and man. However, *Casp1* which is involved in the canonical inflammasome pathway and shown to be activated in fatty livers of mice fed Lieber-DeCarlie diet (22), is not listed as an upregulated gene. *Casp11/4* upregulation is of particular interest as AH is associated with hepatic and systemic bacterial infection initiated by translocation of intestinal bacteria due to dysbiosis and leaky gut (23, 24).

Non-canonical CASP11-GSDMD pathway but not canonical CASP1-IL-1β pathway is activated in AH

To confirm these transcriptome results on inflammasome caspases, we performed immunoblot and qPCR analyses on livers from Control, cASH, and AH mice. Neither pro-CASP1 nor p20 cleaved CASP1 proteins are induced in AH as compared to Control (Fig. 2A). Expected from no CASP1 activation, no evidence of increased pro-IL-1β activation is detected in cASH or AH livers by immunoblot analysis (Fig. 2B). In fact, serum IL-1β levels tend to be lower in AH (Fig. 2C), and liver IL-1β shows no difference in a group of mice subjected to the standard 8-wk AH regimen (AH1) and tends to be reduced even in another group (AH2) which underwent an extended 12-wk AH regimen (Fig. 2D). In contrast, upregulation of pro-CASP11 and active CASP11 are evident in AH (Fig. 3A). *Casp11* mRNA is also upregulated in AH1 and AH2 (Fig. 3B). Further, caspase 11/4 activity in liver homogenate is also significantly increased in AH compared to Control or cASH mice (Fig. 3C). Serum IL-18 levels are increased in both AH1 and AH2 (Fig. 3C). The non-canonical CASP11 activation activates Gasdermin-D (GSDMD) to causes pyroptosis (25). Indeed, the livers from the AH mice but not cASH or Control mice show an appearance of a ~30kD mature GSDMD (Fig. 3E). To test GSDMD activation in a macrophage cell line, Raw264.7 cells were electroporated with an increasing concentration of LPS. With higher concentrations of LPS, mature GSDMD appears and pro-GSDMD is reduced, providing the evidence of GSDMD activation (Fig. 3F). Further, this activation was prevented by the CASP11 inhibitor (Santa Crutz Biotech.), supporting CASP11 is upstream of GSDMD activation (Fig. 3G). To assess the cellular site of GSDMD activation, we have isolated hepatocytes and hepatic macrophages from the AH model and their proteins were immunoblotted with anti-GSDMD antibody. Increased levels of pro-GSDMD are detected in both hepatic macrophages and hepatocytes from the AH mice as compared to the control mice, suggesting a priming effect (Fig. 3H). A cleaved and mature form of GSDMD is also detected clearly in hepatic macrophages from AH and vaguely in hepatocytes (Fig. 3H).

CASP11 deficiency prevents GSDM activation, hepatocyte death, liver bacterial load in AH

To test the causal role of CASP11 *in vivo*, we used the mice which carry a knockout allele of *Casp11* (B6N.129S4(D2)-*Casp4*^{tm1Yuan}/J). This mouse is also defective in CASP1 and pro-IL1β activation. However, since our results showed selective CASP11 activation but not

CASP1 in the AH model, this genetic approach was used to test the role of CASP11 in experimental AH. As shown in Fig. 4A, *Casp11* KO mice are indeed defective in activation of GSDMD in the AH regimen while wild type (WT) mice show GSDMD activation. Although no significant changes are noted in histologic grading for steatosis and inflammation, the incidence of hepatocellular death is suppressed (Fig. 4B, Suppl. Fig. 2) and liver bacterial load as assessed by PCR for the universal bacterial r16S is reduced in *Casp11* KO mice (Fig. 4C). We confirmed decreased hepatocellular death by directly counting hepatocytes which have undergone typical lytic cell death or are still alive to determine the percentage of the death: 1.87± 0.34 in WT AH vs. 0.47 ± 0.04% in Casp11−/− AH, $p<0.01$. Although serum ALT and AST levels are not affected, elevated levels of serum bile acids and alkaline phosphatase are significantly attenuated in *Casp11* KO mice compared to WT mice (Fig. 4D–F). Upregulated *Il17* mRNA levels in the liver of WT AH are markedly attenuated in Casp11−/− AH mouse livers. Conversely, mRNA levels of IL-22 which antagonizes IL-17 expression and has hepatoprotective effects (26), are increased in Casp11−/− AH mice (Fig. 4G).

IL-18 deficiency aggravates GSDMD activation, hepatocyte death, liver bacterial load, and severity of AH

IL-18 was originally identified as a interferon-γ-inducing factor and is generally considered as a proinflammatory cytokine (27). IL-18 deficiency or treatment with anti-IL-18 antiserum protects the mice from acute endotoxemia (28, 29). At the same time, IL-18 serves as one of the most important anti-microbial cytokines and facilitates the early antimicrobial response to E. Coli (30). As IL-18 is upregulated in AH mice (Fig. 3C) concurrent with increased bacterial load (Fig. 4C), we hypothesized that IL-18 deficiency may increase GSDMD activation due to increased bacterial infection. Indeed, in IL-18 KO (IL-18−/−) mice, GSDMD activation and liver bacterial load are all significantly increased (Fig. 5A and C). Concurrently, hepatocyte death and PMN infiltration are increased as assessed by both semi-quantitative morphometry (Fig. 5B, above) and cell number counting (Fig. 5B, below). Intensified PMN infiltration is corroborated by higher hepatic *Myeloperoxidase* (*Mpo*) mRNA levels (Fig. 5D, left). However, Cd68 mRNA expression, the marker for macrophages is reduced in IL-18 KO mice (Fig. 5D, right). Serum ALT, bile acids, and alkaline phosphatase levels are also increased significantly more than WT mice (Fig. 5E and F). Hyalin body inclusion in perivenular hepatocytes are noted in IL-18 KO mice subjected to the AH regimen (arrows, Fig. G-a). Additionally, ductular reaction which is a prognostic indicator for worse AH (31), is also intensified in IL-18 mice (Fig. 5G-b, H&E staining) and confirmed by OV-6 antibody staining (Fig. 5G-c and d). Collectively, these results suggest IL-18 deficiency increases liver bacterial load and GSDMD-mediated pyroptosis of hepatocytes, and worsens AH, the phenotype which is opposite of that observed with *Casp11* KO mice.

Hepatocyte-specific expression of mature GSDM

To directly test the causal role of the mature GSDMD in the model, we overexpressed a N-terminal (aa1-276) active peptide of GSDMD vs. e-GFP as a control using an hepatotrophic AAV-8 serotype vector under the hepatocyte-specific promoter of Ttr (Transthyretin). Mice were injected via tail vein with either vector before the commencement of intragastric

ethanol diet feeding and sacrificed after 8 wk of the AH regimen. Livers of mice injected with AAV-Ttr-mGSDMD show a 4.8-fold increase in *Gsdmd* mRNA compared to those injected with AAV-Ttr-eGFP (Fig. 5A). *Il18* and *Casp11* mRNA are also increased 4-fold and 2-fold, respectively in the GSDMD overexpressing livers compared to those of the AH mice injected with the control virus. Histologically, liver pathology parameters such as macro- or micro-vesicular steatosis are not different between the two groups. However, hepatocyte death and PMN infiltration are significantly increased by GSDMD overexpression (Fig. 5B). Hepatocyte death noted in AAV-Ttr-eGFP-treated mouse livers, involved 1–3 cells surrounded by PMNs in each focus (arrows in Fig. 5C, left panel) whereas multiple hepatocytes exhibited lytic death with more intense PMN infiltration in AAV-Ttr-mGSDMD-injected mouse livers (demarcated by red lines in Fig. 5C, right panels). The counting of dead hepatocytes reveals more than 7% death rate in the AAV-Ttr-mGSDM group as opposed to 1.56±0.76% in the AAV-Ttr-eGFP group (Fig. 6D). Plasma AST levels tend to be higher in GSDMD overexpressing mice ($p=0.07$) resulting in a significant increase in AST/ALT ratio (1.43±0.09 vs. 1.0±0.05, $p<0.05$).

CASP4-GSDMD activation in AH patients

Finally, we tested CASP4-GSDMD activation in the livers from patients with severe AH and healthy donors obtained from the transplant program as described in Methods. Basic characteristics of 5 patients and their clinical information, as well as the age and sex of 5 healthy donors, are summarized in Supplemental Results - Table 5. For these samples, membrane and cytosolic proteins were extracted to help detect active GSDMD in the membrane fraction by immunoblot analysis. Explant livers from 5 patients with clinical and histologic diagnosis of AH (A1-A5), all show a robust increase in cleaved, activated CASP4 in the cytosolic fraction and the appearance of ~30kD mature GSDM in the membrane proteins but not in healthy livers (C1–C5) (Fig. 6F), supporting the activated CASP4-GSDMD pathway in clinical AH.

Discussion

In search for putative drivers responsible for the transition from cASH to AH, we identified the non-canonical inflammasome caspase *CASP11/4* which is upregulated in both mouse and patient AH livers. CASP11/4 cleaves and activates GSDMD to induce programmed lytic cell death called pyroptosis in response to intracellular pathogens and PAMPs (25, 32, 33). Thus, the CASP11/4-GSDMD pathway links bacterial translocation and infection with cellular death. In AH mice with an increased hepatic bacterial load, both CASP11 and GSDMD are activated, but not in cASH livers. CASP11 deficiency abrogates GSDMD activation, hepatocellular death, and liver bacterial load. Conversely, the deficiency of the antimicrobial IL-18, aggravates these parameters and AH in mice. Further, direct overexpression of the mature GSDMD in hepatocytes, increases hepatocyte death and PMN infiltration in the AH model. Finally, the analysis of livers of patients with severe AH vs. healthy controls, confirms that CASP4-GSDMD pathway is activated in clinical AH. Collectively, these results support the novel and pivotal pathogenetic role of the CASP11/4-GSDMD pathway in AH and suggest pyroptosis is a unique form of cell death in AH driven by translocated gut bacteria. Hepatocyes are sensitized or primed by ethanol or secondary

factors to undergo apoptosis caused by activation of intrinsic or extrinsic pro-apoptotic pathways mediated by organelle stress or cytokines (34–36). They may also undergo necroptosis mediated by receptor-interacting protein kinase (RIP) 1-RIP3-mixed lineage kinase domain-like protein (MLKL) activation (36, 37). As apoptosis may suppress necroptosis by caspase-mediated cleavage of RIP3 and the latter cell death is often associated with inflammatory response, apoptosis may occur in early steatotic but not inflammatory stage of ALD followed by necroptosis in ASH. After the transition to AH, pyroptosis may dominate as a form of hepatocellular death mechanistically and consequentially associated with PMN inflammation and endotoxemia/bacteremia (Fig. 7A). Obviously, these different forms of hepatocellular death may co-exist in ALD based on differences in individual cellular state of sensitization/priming and bacterial infection, as well as heterogeneous microenvironment (36).

We also detected activated GSDMD in hepatic macrophages isolated from AH mouse livers. As hepatic macrophages are the first line of defense against translocated bacteria, this can be expected and also has a pathologic significance. It may reduce the macrophage number and compromise local anti-microbial defense, further amplifying a vicious cycle of bacterial infection-pyroptosis-macrophage depletion. Indeed, liver expression of CD68, the marker for macrophages is reduced in AH as compared to cASH (12) and further diminished in AH mice with IL-18 deficiency, always reciprocal to induction of *Mpo*, the marker for PMNs (Fig. 5D). Pyroptosis of infected cells locally disseminates bacteria, PAMP, and DAMP, intensifying PMN infiltration into the hepatic macrophages-depleted liver and worsening AH. With progressive pyroptosis and macrophage depletion, systemic dissemination of bacteria, PAMPS, and DAMPs may cause systemic inflammatory response syndrome (SIRS) and septicemia, the two common life-threatening complications of AH (Fig. 7B). The pro-GSDMD levels were increased in both hepatic macrophages and hepatocytes isolated from the AH model, suggesting the priming of this pyroptotic pathway. The mature form of GSDMD was detected in isolated hepatic macrophages but not readily in hepatocytes. It was technically difficult to detect active GSDMD in hepatocytes most likely because pyroptotic hepatocytes more easily underewent lysis during the isolation procedure. For this reason, we have forced expression of GSDMD in hepatocytes via the AAV vector in the mouse model and demonstrated enhanced hepatocyte death with more intense PMN infiltration.

We have noticed that plasma bile acids and alkaline phosphatase more sensitively responded to the manipulations of CASP11-GSDMD pathway than plasma transaminases (Fig. 4 and 5), suggesting the ductal/ductular effect may be a primary event. In fact, CASP11 deficiency did not rescue hepatic steatosis and inflammation or plasma AST/ALT but reduced these two parameters along with hepatocyte death and liver bacterial load. Indeed, the ductular reaction which is known to correlate with the severity of clinical AH (31), is clearly heightened when CASP11/4-GSDMD activation and liver bacterial load are worsened by IL-18 deficiency. Under such condition, most liver parameters including inflammation and ALT, are coordinately worsened. Endotoxin and inflammatory cytokines are known to induce cholestasis (38, 39). We have previously reported that our AH model has enhanced activation of TLR4 signaling in close association with ductular reaction and upregulation of progenitor genes such as *Cd133* and *Nanog* (12). A most recent study supports a role for LPS-TLR4 pathway in ductular reaction in AH (40). Collectively, these findings suggest

bacterial infection which triggers the CASP11/4-GSDMD pyroptotic pathway in AH may also target the bile duct epithelium to stimulate proliferation of ductular cells/oval cells.

It was surprising that despite the lack of CASP1-mediated canonical inflammasome activation, plasma IL-18 levels were increased in the AH mice. This anti-microbial cytokine might have been processed and activated in extra-hepatic sites. To this end, it is worth noting that human PMNs are shown to constitutively express IL-18 and IL-18-derived moieties via a mechanism mediated by caspase-independent cleavage of pro-IL-18 by the serine proteases, elastase and cathepsin G (41). In fact, in an inflammatory environment, PMNs are a rich source of IL-18 which enhances PMN effector function (42), establishing a functional pivotal positive loop (41).

In summary, the present study disclosed the unique role of the CASP11-GSDMD-pyroptosis pathway in mouse experimental AH and confirmed the activation of this pathway in clinical AH. Our results suggest that the components in this pathway may serve as novel therapeutic targets for AH.

Supplementary Material

Refer to Web version on PubMed Central for supplementary material.

Acknowledgments

The authors thank the Animal Core, Morphology Core, and Administrative Core of the Southern California Research Center for ALPD and Cirrhosis (P50AA011999) for their animal experimental, histological, and administrative services; and Histology Core of USC Research Center for Liver Diseases for tissue processing for paraffin embedding; Molecular Genomics Core and Bioinformatics Core of the USC Norris Comprehensive Cancer Center (P30CA014089) for RNA-seq analysis; and Integrative Liver Cell Core (R24AA012885) for hepatocyte and hepatic macrophage isolation from the AH model. We also thank Dr. Zaoli Sun of Johns Hopkins University for facilitating the availability and use of AH patient and healthy donor livers for this study via the Clinical Resources for Alcoholic Hepatitis Investigators (1R24AA025017). Portions of this research was supported by National Institute of General Medical Sciences of NIH grant P41 GM103493. Proteomics work was performed in W. R. Wiley Environmental Molecular Sciences Laboratory (EMSL), a Department of Energy (DOE) office of Biological and Environmental Research (BER) national user facility located at Pacific Northwest National Laboratory (PNNL). The bioinformatics software and computing resources used in the analysis are funded by the USC Office of Research and the Norris Medical Library.

Supported by grants from NIAAA/NIH: P50AA011999 and R24AA012885 to H.T., R01DK090794 and U01AA021898 to S.W.F., NIGMS/NIH: P41 GM103493 to R.D.S., U01AA021908 to R.B., R01AA020703 and U01AA021856 to B.S., U01AA021884, U01AA021886, and U01AA018389 to T.M. and Medical Research Service of Department of Veterans Affairs to H.T., B.S., T.M.

Abbreviations

CASP11/4	Caspase-11/4
GSDMD	Gasdermin-D
AH	alcoholic hepatitis
ASH	alcoholic steatohepatitis
IL-1β	interleukin-1β
IL-18	interleukin-18

LPS	lipopolysaccharide
mRNA	messenger ribonucleic acid, DNA, deoxyribonucleic acid
PCR	polymerase chain reaction
ELISA	enzyme-linked immunosorbent assay
PMN	polymorphonulear cells
MNC	mononuclear cells
SDS-PAGE	sodium dodecyl sulfate polyacrylamide gel electrophoresis
ALT	alanine aminotransferase
AST	aspartate aminotransferase
AAV	adeno-associated virus
Ttr	transthyretin
PAMP	pathogen associated molecular pattern
DAMP	death associated molecular pattern
SIRS	systemic inflammatory response syndrome

References

1. Lucey MR, Mathurin P, Morgan TR. Alcoholic hepatitis. N Engl J Med. 2009; 360:2758–2769. [PubMed: 19553649]
2. Altamirano J, Miquel R, Katoonizadeh A, Abraldes JG, Duarte-Rojo A, Louvet A, Augustin S, et al. A histologic scoring system for prognosis of patients with alcoholic hepatitis. Gastroenterology. 2014; 146:1231–1239. e1231–1236. [PubMed: 24440674]
3. Thursz MR, Forrest EH, Ryder S, investigators S. Prednisolone or Pentoxifylline for Alcoholic Hepatitis. N Engl J Med. 2015; 373:282–283. [PubMed: 26176387]
4. Mathurin P, Moreno C, Samuel D, Dumortier J, Salleron J, Durand F, Castel H, et al. Early liver transplantation for severe alcoholic hepatitis. N Engl J Med. 2011; 365:1790–1800. [PubMed: 22070476]
5. Lee BP, Chen PH, Haugen C, Hernaez R, Gurakar A, Philosophe B, Dagher N, et al. Three-year Results of a Pilot Program in Early Liver Transplantation for Severe Alcoholic Hepatitis. Ann Surg. 2017; 265:20–29. [PubMed: 27280501]
6. Gao B, Bataller R. Alcoholic liver disease: pathogenesis and new therapeutic targets. Gastroenterology. 2011; 141:1572–1585. [PubMed: 21920463]
7. Mandrekar P, Bataller R, Tsukamoto H, Gao B. Alcoholic hepatitis: Translational approaches to develop targeted therapies. Hepatology. 2016; 64:1343–1355. [PubMed: 26940353]
8. Sugimoto K, Takei Y. Pathogenesis of alcoholic liver disease. Hepatol Res. 2017; 47:70–79. [PubMed: 27138729]
9. Bataller R, Gao B. Liver fibrosis in alcoholic liver disease. Semin Liver Dis. 2015; 35:146–156. [PubMed: 25974900]
10. Xu MJ, Cai Y, Wang H, Altamirano J, Chang B, Bertola A, Odena G, et al. Fat-Specific Protein 27/CIDEC Promotes Development of Alcoholic Steatohepatitis in Mice and Humans. Gastroenterology. 2015; 149:1030–1041 e1036. [PubMed: 26099526]

11. Bertola A, Mathews S, Ki SH, Wang H, Gao B. Mouse model of chronic and binge ethanol feeding (the NIAAA model). Nat Protoc. 2013; 8:627–637. [PubMed: 23449255]
12. Lazaro R, Wu R, Lee S, Zhu NL, Chen CL, French SW, Xu J, et al. Osteopontin deficiency does not prevent but promotes alcoholic neutrophilic hepatitis in mice. Hepatology. 2015; 61:129–140. [PubMed: 25132354]
13. Ueno A, Lazaro R, Wang PY, Higashiyama R, Machida K, Tsukamoto H. Mouse intragastric infusion (iG) model. Nat Protoc. 2012; 7:771–781. [PubMed: 22461066]
14. Affo S, Dominguez M, Lozano JJ, Sancho-Bru P, Rodrigo-Torres D, Morales-Ibanez O, Moreno M, et al. Transcriptome analysis identifies TNF superfamily receptors as potential therapeutic targets in alcoholic hepatitis. Gut. 2013; 62:452–460. [PubMed: 22637703]
15. Kim D, Pertea G, Trapnell C, Pimentel H, Kelley R, Salzberg SL. TopHat2: accurate alignment of transcriptomes in the presence of insertions, deletions and gene fusions. Genome Biol. 2013; 14:R36. [PubMed: 23618408]
16. Mudge JM, Harrow J. Creating reference gene annotation for the mouse C57BL6/J genome assembly. Mamm Genome. 2015; 26:366–378. [PubMed: 26187010]
17. Bullard JH, Purdom E, Hansen KD, Dudoit S. Evaluation of statistical methods for normalization and differential expression in mRNA-Seq experiments. BMC Bioinformatics. 2010; 11:94. [PubMed: 20167110]
18. Dautel SE, Kyle JE, Clair G, Sontag RL, Weitz KK, Shukla AK, Nguyen SN, et al. Lipidomics reveals dramatic lipid compositional changes in the maturing postnatal lung. Sci Rep. 2017; 7:40555. [PubMed: 28145528]
19. Wang L, Fouts DE, Starkel P, Hartmann P, Chen P, Llorente C, DePew J, et al. Intestinal REG3 Lectins Protect against Alcoholic Steatohepatitis by Reducing Mucosa-Associated Microbiota and Preventing Bacterial Translocation. Cell Host Microbe. 2016; 19:227–239. [PubMed: 26867181]
20. Schwanhausser B, Busse D, Li N, Dittmar G, Schuchhardt J, Wolf J, Chen W, et al. Global quantification of mammalian gene expression control. Nature. 2011; 473:337–342. [PubMed: 21593866]
21. Jorgensen I, Miao EA. Pyroptotic cell death defends against intracellular pathogens. Immunol Rev. 2015; 265:130–142. [PubMed: 25879289]
22. Petrasek J, Bala S, Csak T, Lippai D, Kodys K, Menashy V, Barrieau M, et al. IL-1 receptor antagonist ameliorates inflammasome-dependent alcoholic steatohepatitis in mice. J Clin Invest. 2012; 122:3476–3489. [PubMed: 22945633]
23. Yan AW, Fouts DE, Brandl J, Starkel P, Torralba M, Schott E, Tsukamoto H, et al. Enteric dysbiosis associated with a mouse model of alcoholic liver disease. Hepatology. 2011; 53:96–105. [PubMed: 21254165]
24. Chen P, Torralba M, Tan J, Embree M, Zengler K, Starkel P, van Pijkeren JP, et al. Supplementation of saturated long-chain fatty acids maintains intestinal eubiosis and reduces ethanol-induced liver injury in mice. Gastroenterology. 2015; 148:203–214 e216. [PubMed: 25239591]
25. Kayagaki N, Stowe IB, Lee BL, O'Rourke K, Anderson K, Warming S, Cuellar T, et al. Caspase-11 cleaves gasdermin D for non-canonical inflammasome signalling. Nature. 2015; 526:666–671. [PubMed: 26375259]
26. Lafdil F, Miller AM, Ki SH, Gao B. Th17 cells and their associated cytokines in liver diseases. Cell Mol Immunol. 2010; 7:250–254. [PubMed: 20305686]
27. Akira S. The role of IL-18 in innate immunity. Curr Opin Immunol. 2000; 12:59–63. [PubMed: 10679398]
28. Hochholzer P, Lipford GB, Wagner H, Pfeffer K, Heeg K. Role of interleukin-18 (IL-18) during lethal shock: decreased lipopolysaccharide sensitivity but normal superantigen reaction in IL-18-deficient mice. Infect Immun. 2000; 68:3502–3508. [PubMed: 10816504]
29. Netea MG, Fantuzzi G, Kullberg BJ, Stuyt RJ, Pulido EJ, McIntyre RC Jr, Joosten LA, et al. Neutralization of IL-18 reduces neutrophil tissue accumulation and protects mice against lethal Escherichia coli and Salmonella typhimurium endotoxemia. J Immunol. 2000; 164:2644–2649. [PubMed: 10679104]

30. Weijer S, Sewnath ME, de Vos AF, Florquin S, van der Sluis K, Gouma DJ, Takeda K, et al. Interleukin-18 facilitates the early antimicrobial host response to Escherichia coli peritonitis. Infect Immun. 2003; 71:5488–5497. [PubMed: 14500466]

31. Sancho-Bru P, Altamirano J, Rodrigo-Torres D, Coll M, Millan C, Jose LJ, Miquel R, et al. Liver progenitor cell markers correlate with liver damage and predict short-term mortality in patients with alcoholic hepatitis. Hepatology. 2012; 55:1931–1941. [PubMed: 22278680]

32. Ding J, Wang K, Liu W, She Y, Sun Q, Shi J, Sun H, et al. Pore-forming activity and structural autoinhibition of the gasdermin family. Nature. 2016; 535:111–116. [PubMed: 27281216]

33. Liu X, Zhang Z, Ruan J, Pan Y, Magupalli VG, Wu H, Lieberman J. Inflammasome-activated gasdermin D causes pyroptosis by forming membrane pores. Nature. 2016; 535:153–158. [PubMed: 27383986]

34. Kurose I, Higuchi H, Miura S, Saito H, Watanabe N, Hokari R, Hirokawa M, et al. Oxidative stress-mediated apoptosis of hepatocytes exposed to acute ethanol intoxication. Hepatology. 1997; 25:368–378. [PubMed: 9021949]

35. Ji C, Kaplowitz N. Betaine decreases hyperhomocysteinemia, endoplasmic reticulum stress, and liver injury in alcohol-fed mice. Gastroenterology. 2003; 124:1488–1499. [PubMed: 12730887]

36. Wang S, Pacher P, De Lisle RC, Huang H, Ding WX. A Mechanistic Review of Cell Death in Alcohol-Induced Liver Injury. Alcohol Clin Exp Res. 2016; 40:1215–1223. [PubMed: 27130888]

37. Roychowdhury S, McMullen MR, Pisano SG, Liu X, Nagy LE. Absence of receptor interacting protein kinase 3 prevents ethanol-induced liver injury. Hepatology. 2013; 57:1773–1783. [PubMed: 23319235]

38. Kyokane T, Norimizu S, Taniai H, Yamaguchi T, Takeoka S, Tsuchida E, Naito M, et al. Carbon monoxide from heme catabolism protects against hepatobiliary dysfunction in endotoxin-treated rat liver. Gastroenterology. 2001; 120:1227–1240. [PubMed: 11266386]

39. Li N, Choudhuri S, Cherrington NJ, Klaassen CD. Down-regulation of mouse organic anion-transporting polypeptide 4 (Oatp4; Oatp1b2; Slc21a10) mRNA by lipopolysaccharide through the toll-like receptor 4 (TLR4). Drug Metab Dispos. 2004; 32:1265–1271. [PubMed: 15483194]

40. Odena G, Chen J, Lozano JJ, Altamirano J, Rodrigo-Torres D, Affo S, Morales-Ibanez O, et al. LPS-TLR4 Pathway Mediates Ductular Cell Expansion in Alcoholic Hepatitis. Sci Rep. 2016; 6:35610. [PubMed: 27752144]

41. Robertson SE, Young JD, Kitson S, Pitt A, Evans J, Roes J, Karaoglu D, et al. Expression and alternative processing of IL-18 in human neutrophils. Eur J Immunol. 2006; 36:722–731. [PubMed: 16506286]

42. Leung BP, Culshaw S, Gracie JA, Hunter D, Canetti CA, Campbell C, Cunha F, et al. A role for IL-18 in neutrophil activation. J Immunol. 2001; 167:2879–2886. [PubMed: 11509635]

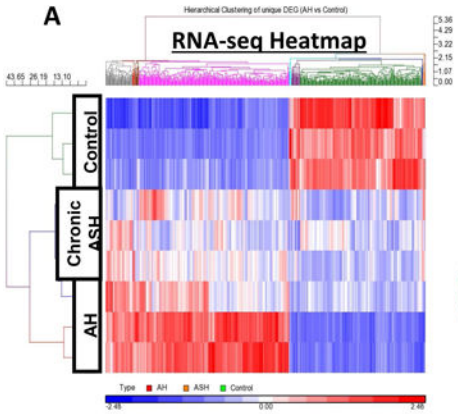

C

The disease and functional categories of upregulated genes common in AH mice and patients vs. respective controls

Name	p-value	# Molecules
Cancer	7.68E-34 - 4.55E-07	534
Cardiovascular Disease	1.02E-28 - 2.06E-07	125
Inflammatory Response	3.16E-28 - 4.73E-07	181
Organismal Injury and Abnormalities	3.60E-20 - 4.55E-07	372
Immunological Disease	1.00E-18 - 1.23E-07	156

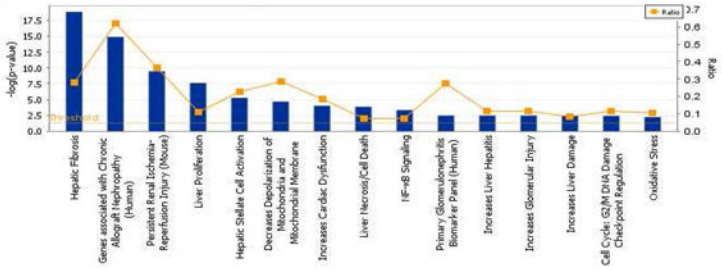

D

The disease and functional categories of down-regulated genes common in AH mice and patients as compared to respective controls.

Name	p-value	# Molecules
Developmental Disorder	1.29E-22 - 1.06E-02	35
Hereditary Disorder	1.29E-22 - 9.80E-03	65
Metabolic Disease	1.29E-22 - 9.86E-03	90
Organismal Injury and Abnormalities	3.39E-13 - 9.80E-03	94
Renal and Urological Disease	3.39E-13 - 1.88E-03	25

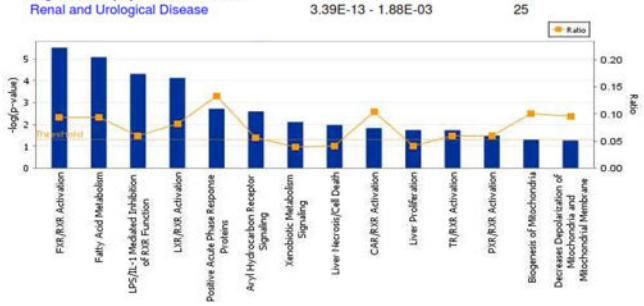

E

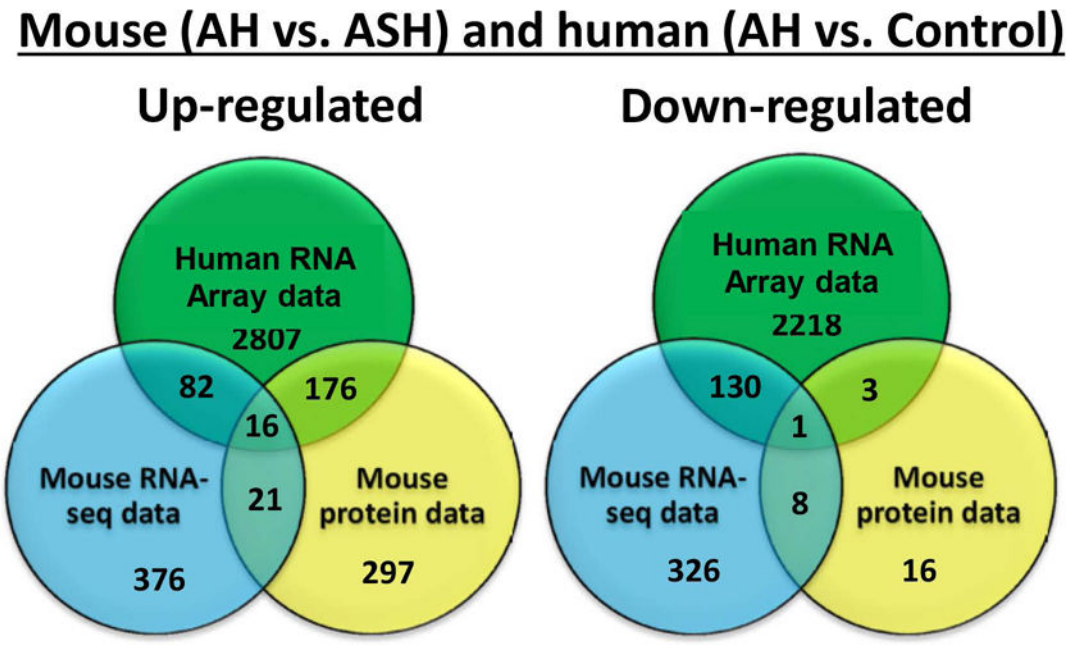

Fig. 1.

A. RNA-seq heatmap for livers from Control, chronic ASH and AH mice. B. Venn diagrams depict differentially regulated genes and proteins in mouse AH livers vs. Control mouse livers as compared to differentially regulated genes in human AH livers vs. healthy livers. C. Ingenuity pathway analysis showing the five most affected functional categories of upregulated genes common in AH mice and patients compared to respective controls. D. The functional categories of downregulated genes common in AH mice and patients compared to respective controls. E. Differentially regulated genes in AH mice vs. chronic ASH mice are compared to differentially regulated genes in AH patient livers vs. healthy livers as depicted by Venn diagrams.

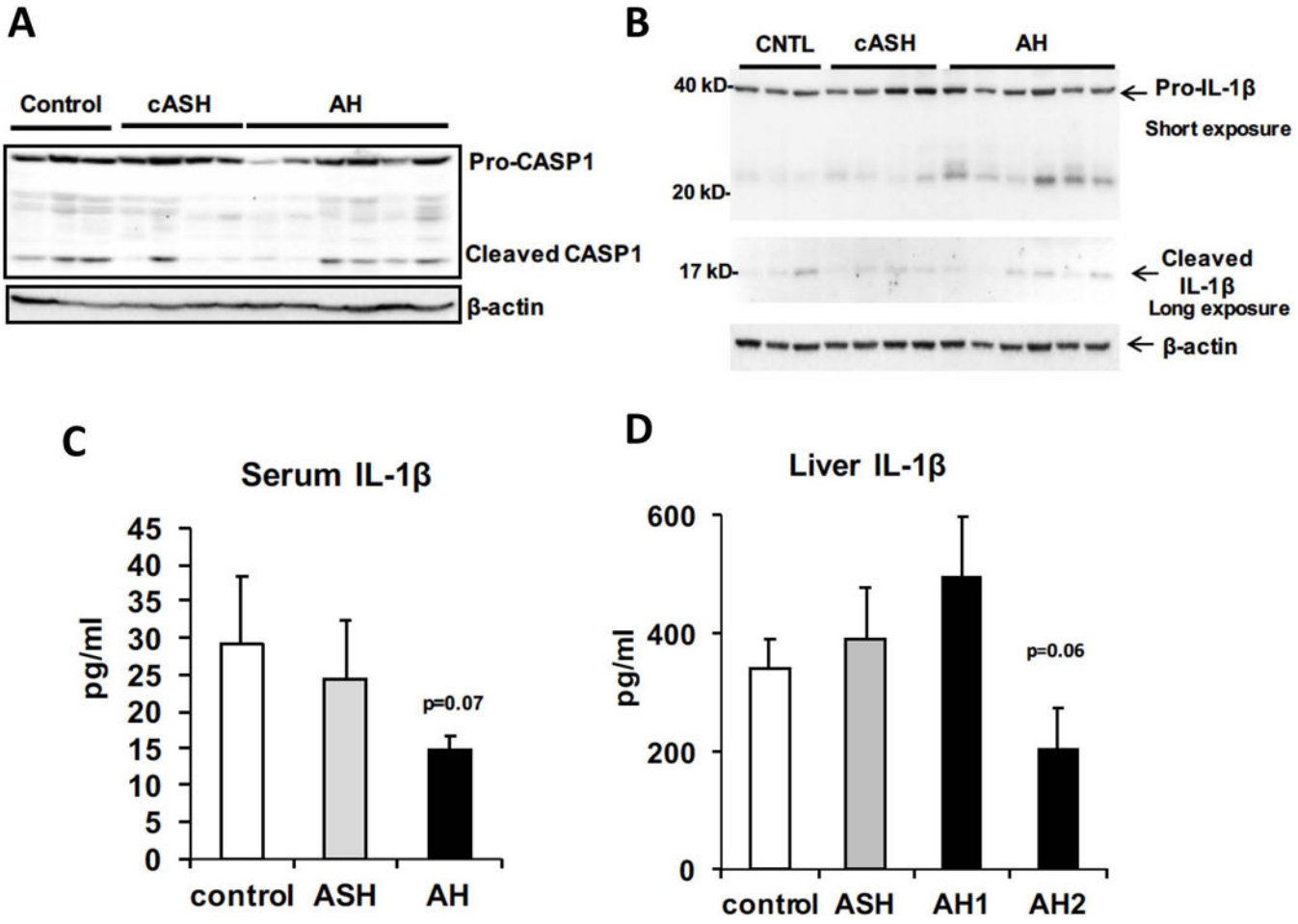

Fig. 2.

A. CASP1 immunoblotting of liver protein extracts from Control, chronic ASH (cASH) and AH mice. B. IL-1β immunoblotting of liver protein extracts from the same three groups of mice. C. Serum IL-1β levels determined by ELSA. D. IL-1β levels in liver homogenate supernatant (50mg liver/ml) determined by ELISA. AH1 and AH2 are cohorts of AH mice subjected to 8-wk and 12 wk regimen, respectively.

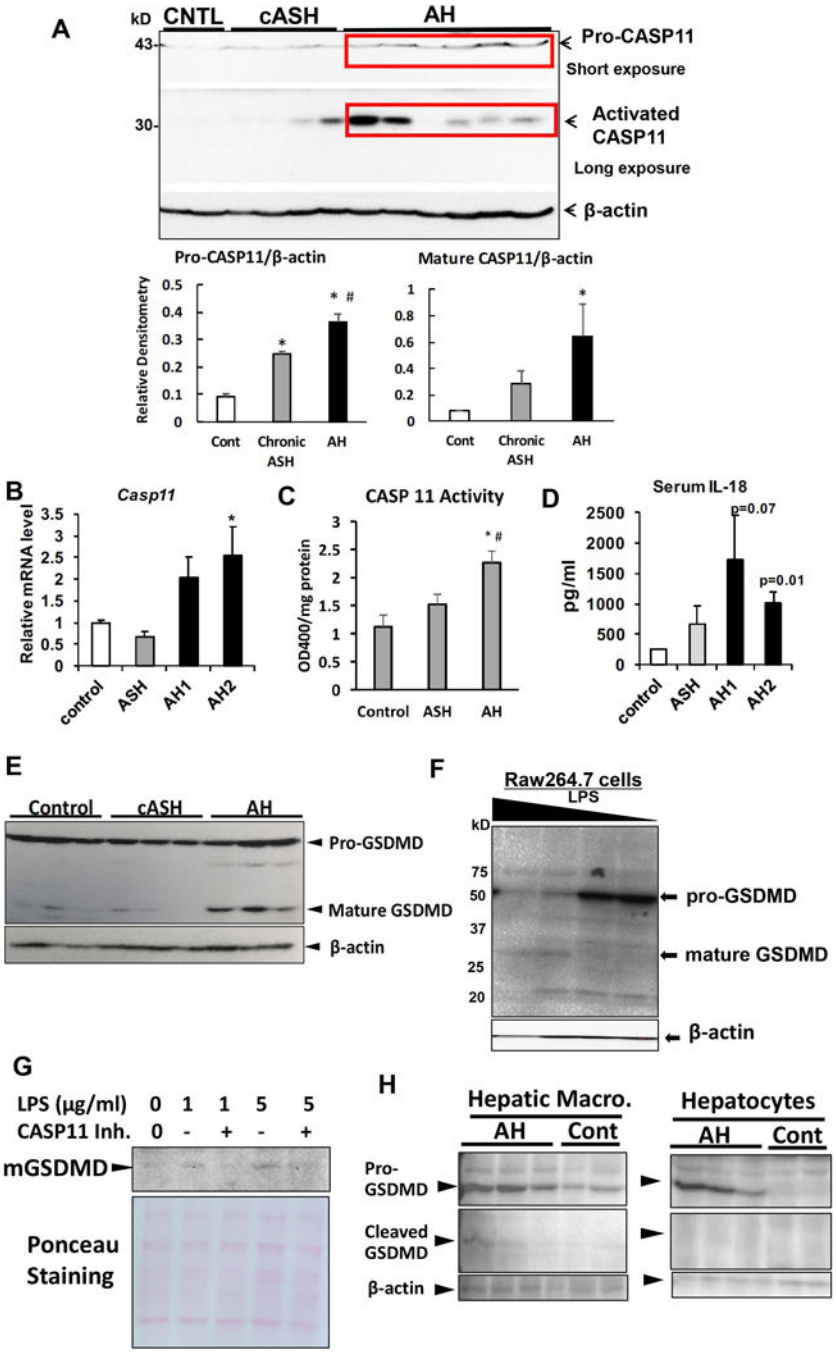

Fig. 3.

A. CASP11 immunoblotting of liver protein extracts from Control (CNTL), chronic ASH (cASH), and AH mice. Densitometry data for pro-CASP11 and mature CASP11 are shown below after standardization to β-actin. *p<0.05 vs. CNTL; #p<0.05 vs. cASH. B. Casp11 mRNA levels in the livers of CNTL, ASH, and two AH cohort mice as described for Fig. 2C. *p<0.05 vs. Control. C. CASP11 activity in livers of Control, ASH and AH mice. D. Serum IL-18 levels determined by ELISA. P values shown are as compared to Control. E. GSDMD immunoblotting of protein extracts from the livers of Control, cASH and AH mice.

F. GSDMD immunoblotting of protein extracts from Raw264.7 cells electroporated with an increasing concentration of LPS (0.125~4μg/ml). G. The CASP11 inhibitor (Santa Cruz Biotech., 30μM) prevents GSDMD activation in Raw264.7 cells electroporated with LPS (1 or 5 μg/ml) as demonstrated by immunoblot anlaysis of membraine proteins. Ponceau staining below shows equal proteon loading. H. GSDMD immunoblotting of hepatic macrophages or hepatocytes isolated from the AH or control mice.

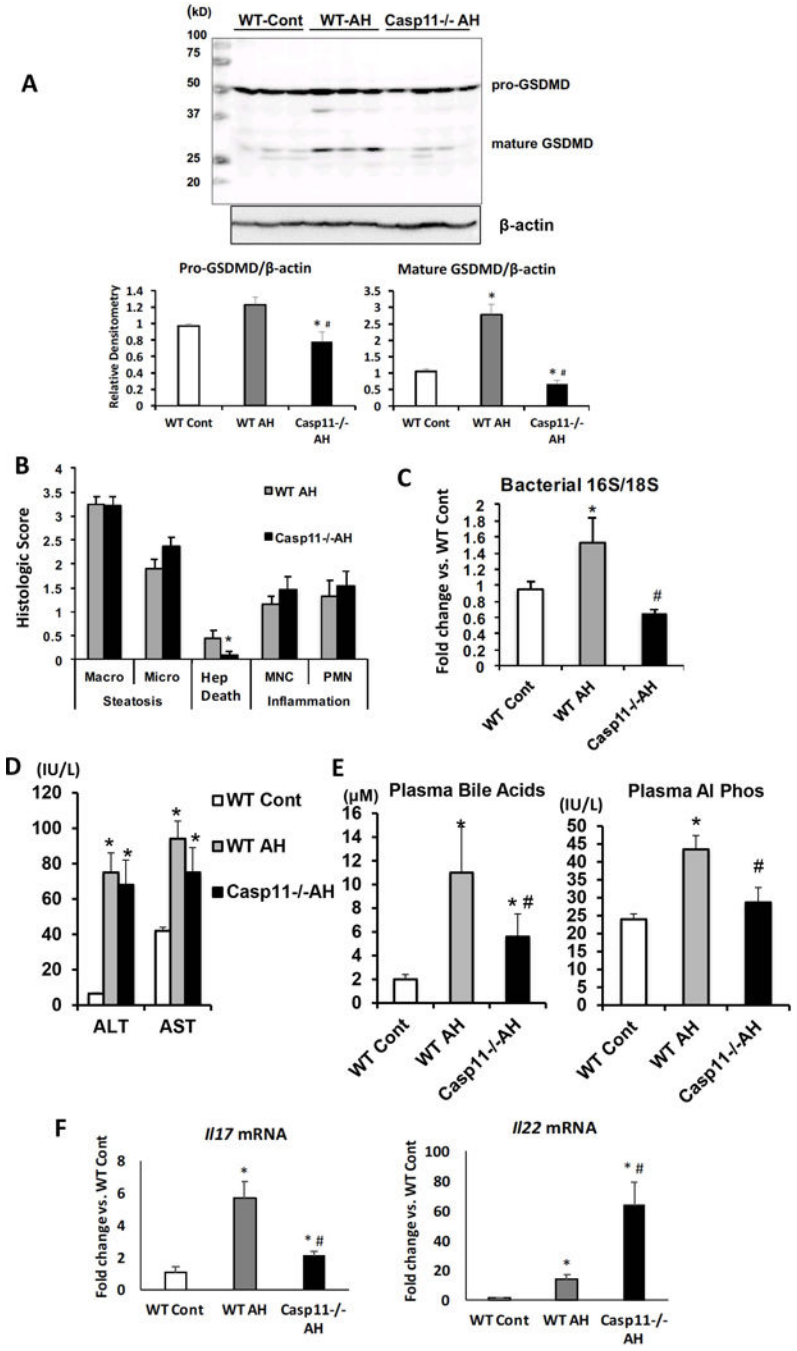

Fig. 4.

A. GSDMD immunoblotting of liver proteins from wild type (WT)-control, WT-AH, and Casp11 KO-AH mice. Densitometry data for pro- and mature GSDMD are shown below after standardization to β-actin. *p<0.05 vs. WT-Cont; #p<0.05 vs. WT-AH. B. Liver histological grading of WT-AH and Casp11KO-AH (Casp11−/−AH) mice as assessed by the evaluation criteria described in Methods. *p<0.05 vs. WT-AH. C. Hepatic bacterial r16S data standardized by host r18S PCR data for WT-Cont, WT-AH, and Casp11−/− AH livers. *p<0.05 vs. WT-Cont; #p<0.05 vs. WT-AH. D. Plasma ALT and AST levels of WT-Cont,

WT-AH, and Casp11−/− AH mice. *p<0.05 vs. WT-Cont. E. Plasma bile acids and alkaline phosphatase levels. *p<0.05 vs. WT-Cont; #p<0.05 vs. WT-AH. F. Liver *Il17a* or *Il22* mRNA levels. *p<0.05 vs. WT-Cont; #p<0.05 vs. WT-AH.

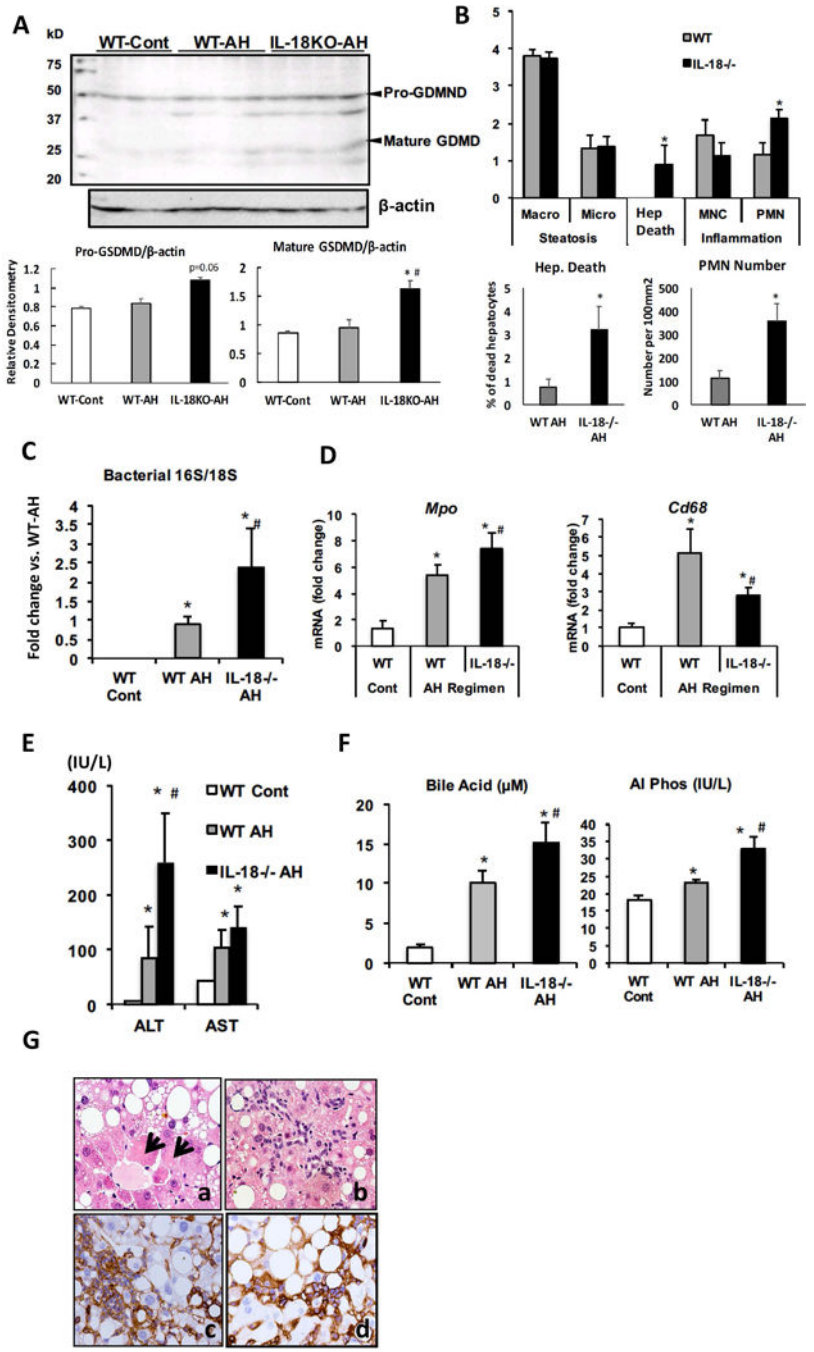

Fig. 5.

A. GSDMD immunoblotting of liver proteins from AT-Cont, WT-AH, and IL18KO-AH. Densitometry data are shown below after standardization to β-actin. p=0.05 or *p<0.05 vs. WT-Cont; #p<0.05 vs. WT-AH. B. Liver histological grading (above). *p<0.05 vs. WT. The percentage of hepatocytes undergoing lytic death and the number of infiltrating PMNs as determined by cell counting (below). *p<0.05 vs. WT-AH. C. Liver bacterial r16S/host r18S PCR data. *p<0.05 vs. WT-Cont; #p<0.05 vs. WT-AH. D. Liver myeloperoxidase (Mop) and Cd68 mRNA levels. *p<0.05 vs. WT-Cont.; #p<0.05 vs. WT-AH. E. Plasma ALT and AST

levels. *p<0.05 vs. WT-Cont; #p<0.05 vs. WT-AH. F. Plasma bile acid and alkaline phosphatase levels. *p<0.05 vs. WT-Cont; #p<0.05 vs. WT-AH. G. An upper-left photo of H&E staining of IL18−/− AH liver showing intracellular hyaline inclusion in hepatocytes (a, arrows). Ductular reactions by H&A staining (b) and by immunostaining with OV-6 antibody (c and d) depicting the presence of oval cells (progenitors) consisting of ductular reactions.

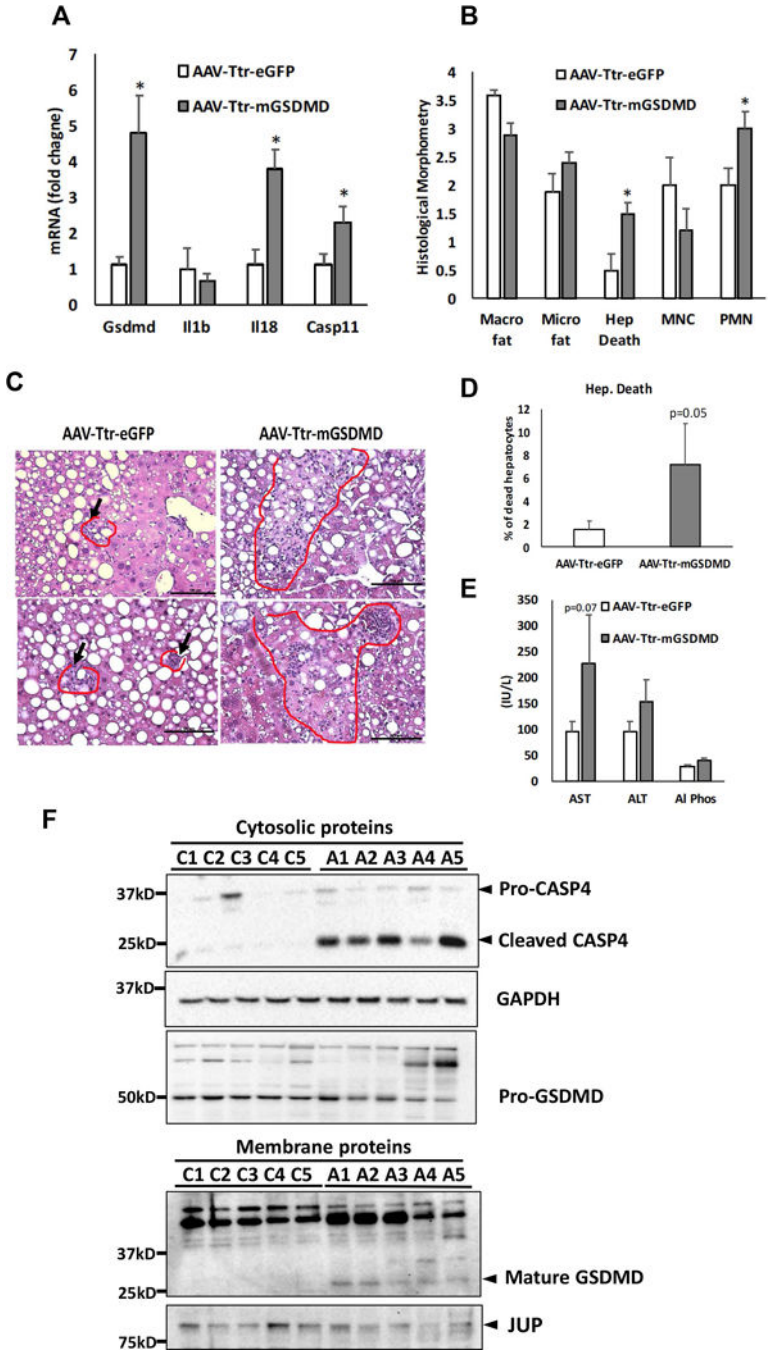

Fig. 6.

A. Liver mRNA levels of *Gsdmd*, *Il1b*, *Il18*, *Casp11* of WT mice injected via tail vain with AAV-Ttr-eGFP vs. AAV-Trt-mGSDMD (5×10e11 GC/mouse) and subjected to the 8-wk AH regimen. *p<0.05 vs. AAV-Ttr-eGFP-injected mice. B. Liver histological grading of the two groups of mice described for Fig. 6A. *p<0.05 vs. AAV-Ttr-eGFP-injected mice. C. Representative photomicrographs of H&E stained livers of AAV-Ttr-eGFP or AAV-Ttr-mGSDMD-injected mice described above. Black arrows and red circles on left two photos, indicate the foci of 1–3 lytic dead hepatocytes surrounded by PMNs in the AAV-Trt-eGFP

mice. Right two photos depict clusters of multiple lytic hepatocytes in AAV-Ttr-mGSDMD-injected mouse livers with more intense PMN infiltration. A black bar = 50μm. D. Lytic dead hepatocytes were counted and expressed as the percent of total hepatocytes as described in Methods. E. Plasma AST, ALT and alkaline phosphatase levels of the two groups of mice described above. F. Immunoblot analysis of cytosolic and membrane fractions of AH patient (A1-5) or healthy donor (C1-5) livers for CASP4 and GSDMD. As loading controls for cytosol and membrane proteins, GAPDH and JUP (junction plakoglobin) were immunoblotted, respectively.

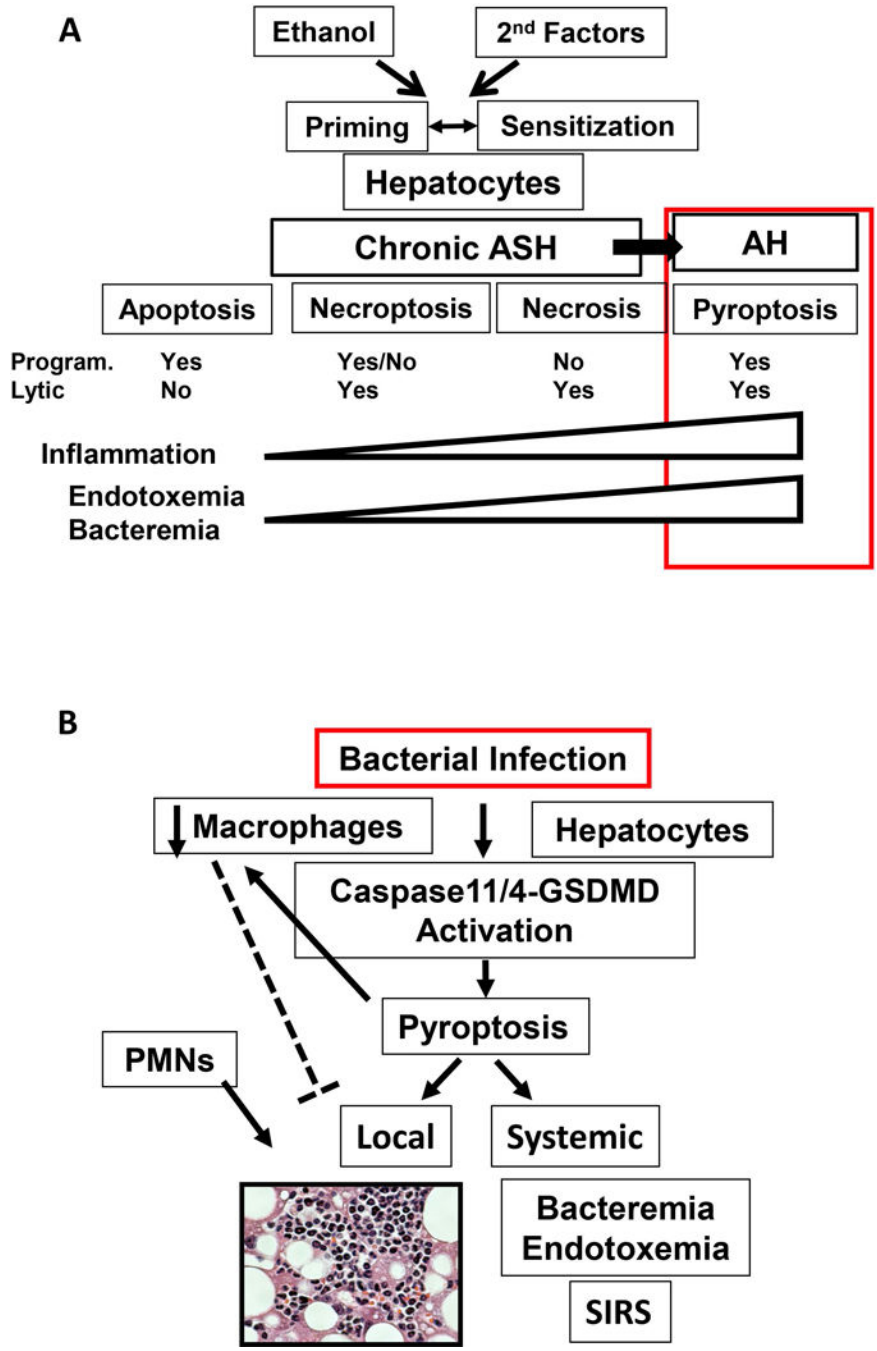

Fig. 7.

A. A schematic diagram of the proposed role of pyroptotic cell death of hepatocytes in the transition from chronic ASH to AH accompanied by increased bacterial load and PMN inflammation. B. A schematic diagram of how pyroptosis of hepatic macrophages diminishes local defense and necessitates more intense PMN infiltration to respond to bacteria or DAMP released by pyroptotic cell death. If excessive, bacteria or DANP released by pyroptosis may systemically lead to bacteremia, endotoxemia and SIRS.

Table 1

Ontology and pathway analysis of 98 up-regulated AH vs. ASH genes common in the mouse model and patients (the genes are repeated in different categories).

Functions	Gene symbols	# Genes
Chemokine signaling	CCR2, CD47, COL4A3, CXCL5, FCER1G, CAPG, ITGA6, ITGB2, MMP7, PLAU, S100A4, SIRPA, SPP1, TGFBR1, TRPM4, COL4A3, ITGA6, TGFBR1, FGF21	19
Inflammasome activation	**CASP11/4**, FCER1G, ITGB2, ALCAM, GPX2, CCR2, CD47, LPL, ANXA4, SLPI, IQGAP1, TRPM4, VTCN1, DYNLL1, RAP1GAP, CFTR, CAPG	17
Exosome formation	TSPAN8, CXCL5, CD53,ITGB2,ITGB6, FGF21,FGFR2, PLAU, S100A4, SPP1, STMN1, TGFBR1, LTBP2, MSN, SERPINE2, FCER1G, PLAT, AKR1B10, VCAN, SVEP1, GOLM1, TESC	22
Cell migration	ANXA3, CAPG, CCR2, CD47, CFTR, COL4A3, CXCL5, DDR1, EHF, F13A1, FCER1G, FGFR2, IQGAP1, ITGA6, ITGB2, ITGB6, LAMC2, LTBP2, MMP7, MSN, PLAT, PLAU, RAP1GAP, RAP2B, S100A4, SERPINE2, SIRPA, SLPI, SPP1, STMN1, TGFBR1, TRPM4, VCAN, VTCN1	35
Cells invasion	ALCAM, CD53, IQGAP1, ITGA6, ITGB6, MARCKS, PLAT, PLAU, RAP1GAP, S100A4, S100A6, SERPINE2, SOX4, SPP1, ST14, STMN1, TGFBR1, UBD, VCAN, WISP2	20
Phagocytosis	ANXA3, CAPG, CD47, FCER1G, ITGB2, MSN, PLAU, SIRPA	8
Bacterial Infection	CAPG, **CASP11/4**, CCR2, CD47, CFTR, CXCL5, FCER1G, FGFR2, GABRP, GCA, ITGB2, LTBP2, MMP7, SIRPA, SLPI, SPP1, TLR1, TOP2A, UBD, VTCN1	20
Fibrosis	CCR2, CFTR, COL4A3, FGFR2, GOLM1, LPL, MMP7, PKHD1, PLAT, PLAU, S100A4, SLC7A11, SPP1, STMN1, TGFBR1, UBD	16
Cell proliferation	AKR1B10, ALCAM, CCR2, CD47, CDKN3, COL4A3, CXCL5, DDR1, EHF, FCER1G, FGF21, FGFR2, GABRP, GOLM1, IQGAP1, ITGA6, ITGB2, LAIR1, MARCKS, MKI67, MMP7, PCNA, PFKP, PKHD1, PLAT, PLAU, RAP1GAP, RBM3, S100A4, S100A6, SERPINE2, SIRPA, SLC7A11, SLPI, SOX4, SPP1, STMN1, TESC, TGFBR1, THG1L, TOP2A, TRPM4, VCAN, VTCN1, WISP2	45
Metastasis	ALCAM, CAPG, CCR2, CD47, CXCL5, FGFR2, FRY, ITGA6, MMP7, PLAT, PLAU, S100A4, SLC7A11, SPP1, TGFBR1, TOP2A, VTCN1	17
Cell necrosis	ALCAM, CASP4, CCR2, CD47, COL4A3, DYNLL1, EHF, F13A1, FCER1G, FGFR2, FUBP1, GABRP, GPX2, ITGA6, ITGB2, LAIR1, MMP7, MSN, PCNA, PLAT, PLAU, RAB32, RAP1GAP, S100A4, S100A6, SERPINE2, SIRPA, SLC7A11, SLPI, SOX4, SPP1, ST14, STMN1, TGFBR1, TLR1, TOP2A, TRPM4, UBD, VCAN	39
Apoptosis	ALCAM, ANXA4, CASP4, CCR2, CD47, CD53, COL4A3, DDR1, DYNLL1, EHF, F13A1, FCER1G, FGFR2, FUBP1, GABRP, GPX2, ITGA6, ITGB2, LAIR1, MLLT11, MMP7, MSN, PCNA, PKHD1, PLAT, PLAU, RAB32, RAP1GAP, S100A4, S100A6, SERPINE2, SIRPA, SLC7A11, SLPI, SOX4, SPINT1, SPP1, ST14, STMN1, TGFBR1, THG1L, TLR1, TOP2A, TRPM4, UBD, VCAN, VTCN1	47